ARTICLE

Unraveling topology-induced shape transformations in dendrimersomes[†],[**]

Nina Yu. Kostina,[a],[‡] Anna M. Wagner,[a],[‡] Tamás Haraszti,[a] Khosrow Rahimi,[a] Qi Xiao,[b, c] Michael L. Klein,[c] Virgil Percec,[b] and Cesar Rodriguez-Emmenegger [a],*

In memory of William Stebniki Tabora

The vital functions of cell membranes require their ability to quickly change shape to perform complex tasks such as motion, division, endocytosis, and apoptosis. Membrane curvature in cells is modulated by very complex processes such as changes in lipid composition, the oligomerization of curvature-scaffolding proteins, and the reversible insertion of protein regions that act like wedges in the membrane. But, could much simpler mechanisms support membrane shape transformation? In this work, we demonstrate how the change of amphiphile topology in the bilayer can drive shape transformations of cell membrane models. To tackle this, we have designed and synthesized new types of amphiphiles —Janus dendrimers— that self-assemble into uni-, multilamellar, or smectic-ordered vesicles, named dendrimersomes. We synthesized Janus dendrimers containing a photo-labile bond that upon UV-Vis irradiation cleavage loses a part of the hydrophilic dendron. This leads to a change from a cylindrically to a wedge-shaped amphiphile. The high mobility of these dendrimers allows for the concentration of the wedge-shaped amphiphiles and the generation of transmembrane asymmetries. The concentration of the wedges and their rate of segregation allowed control of the budding and generation of structures such as tubules and high genus vesicles.

Introduction

One of the most significant traits of cell membranes is their fluidity and flexibility allowing cells to achieve a multitude of shapes and morphological transformations.[1, 2] The shape of biological membranes determines the morphology of cells and their organelles.[3] Furthermore, the generation of highly curved membrane morphologies plays a vital role in a plethora of cellular functions such as feeding, signal transduction, intra- and extracellular vesicle trafficking, division, motility, apoptosis, and various killing strategies based on defensin-like antimicrobial peptides.[1, 4, 5] *In vivo* the shape of membranes is dynamically modulated and maintained by various passive (exergonic) and active mechanisms involving changes in lipid composition, clustering of wedge-shaped transmembrane proteins, protein crowding, scaffolding by oligomerized peripheral membrane proteins such as clathrin and caveolins, or by force-generating systems such as dynamin rings, Z-rings, ESCRTs or the

polymerization of cytoskeletal proteins and microtubule motor activity.[1, 3, 4, 6-8] Moreover, lipids and proteins can diffuse across the membrane and form distinct lateral domains that segregate molecules with similar characteristics into clusters that differ from the surrounding membrane, the raft domains, associated with highly advanced membrane functions.[9-13] The enormous complexity of living cells and the simultaneous interplay of phenomena makes the understanding of shape transformation in living organism an incredibly difficult feat, even for the simplest minimal cells.[14, 15]

On the other hand, there is a substantial amount of theoretical and experimental work probing the conditions for reshaping of giant unilamellar vesicles (GUV) formed from the self-assembly of lipids and amphiphilic di- and triblock copolymers into liposomes and polymersomes.[16-26] The liposomes display the same thickness, and similar flexibility and fluidity as cell membranes but offer a much lower stability as characterized by the energy stored at break. However, polymersomes have an increased stability but in general, their membrane is much thicker than natural membranes and their fluidity is stalled by the entanglement of the hydrophobic chains even above the glass transition of the hydrophobic block.[22, 27, 28] Thus, liposomes are currently the most well-established model to study bilayer membrane properties.[16-21]

These GUVs exhibit fascinating morphologies encompassing spheres, prolates, dumbbells, pears, stomatocytes, and even complex high genus vesicles.[29-34] For vesicles where flip-flop is allowed, the polymorphism of vesicles observed on the micrometer scale can be understood in terms of curvature models, which depend on two geometric parameters, and two material parameters. The geometric parameters include

a. *DWI- Leibniz Institute for Interactive Materials, Forckenbeckstraße 50, 52074 Aachen, Germany. E-mail: rodriguez@dwi.rwth-aachen.de*
b. *Roy & Diana Vagelos Laboratories, Department of Chemistry, University of Pennsylvania, Philadelphia, PA 19104-6323, United States.*
c. *Institute of Computational Molecular Science, Temple University, Philadelphia, PA 19122, United States.*
‡Both authors contributed equally to this manuscript.

volume (V) and area (A) of the vesicle. However, the shape transformations are mostly governed by bending deformations, that depend on the material parameters: the spontaneous curvature (m, a local term), which represents the preferred curvature of the membrane and reflects the asymmetry between the two leaflets of the bilayer, and its bending rigidity, which describes the resistance of the membrane to bend away from the preferred curvature. On the other hand, if flip-flop is negligible in the experimental timescales, the spontaneous curvature model has to be supplemented by an additional non-local term.[35-38] In this situation, the difference in the number of amphiphiles between the leaflets is constant and leads to a preferred area difference between them (A_0^{in} or A_0^{out}). Initially this constraint was integrated into the bilayer-coupling model[32, 38, 39] and then extended to the area-difference-elasticity model (ADE).[34, 35, 40] It is noteworthy, that all the stationary shapes of the ADE model are also stationary shapes in the spontaneous curvature model using an effective curvature $m_{eff} \equiv m + m_{nlo}$, where m_{nlo} is the non-local spontaneous curvature, which accounts for the fact that the areas of individual leaflets are not constant but can have actual areas (A^{in} or A^{out}) which can differ from the preferred areas at the expense of elastic energy consumption.[34, 35]

Remarkably, vesicles are extremely sensitive to transmembrane asymmetries.[31, 34, 41, 42] The controlled remodeling demands to couple an external stimulus with one of these membrane parameters. Variations of the osmotic balance[43] and changing the permeability of the membranes have been used as a trigger to change V. Stimuli to change A include temperature changes,[34] fusion with micelles to expand the area,[44] photoswitches that expand the packing,[45] and insertion of macromolecular amphiphiles in a single leaflet.[42] However, the highest sensitivity to changes relies on changing m and the differential area. This has been achieved by introducing transmembrane redistribution of lipids in an amount as small as 0.1%,[41] changing the topology of lipids by chemical reactions[46-48] or photoswitching,[49, 50] and by the insertion of peptides and transmembrane proteins.[51] Furthermore, m can be changed by changing the packing of the head groups or exerting a new force by an electric field,[52] the adsorption or depletion of ions,[53, 54] non-charged molecules, polymers (brush and mushroom conformations),[55, 56] proteins,[15, 57] nanoparticles,[58-60] and even living bacteria.[61]

But what is the origin of m in the absence of external stimuli? The elastic models tacitly assume that lipids constitute a smooth structureless elastic interface.[62] However, such a smooth interface does not persist at the molecular scale.[1, 63] At this scale, the lipids undergo in-plane and orthogonal thermal displacement and rotational motion around their vertical axes. These displacements generate molecular protrusions which are only visible at small space and time scales.[63] Moreover, because membranes are many-particle systems, the intermolecular interactions build up to produce cooperative phenomena, *i.e.* the lipids feel each other at much longer ranges defined by the coherence length. Thus, changes in the topology of only a small ratio of the lipids that affect their motion modes propagate over much larger scales across the bilayer and cause fluctuations in the composition, packing, bending rigidity that extend from the nm- to the μm-range. Such profound changes manifest in the change of m.
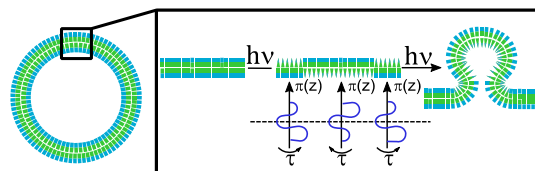

Fig. 1. Schematic representation of curvature generation in the bilayer membrane by changing the topology of the amphiphile molecules. By applying a specific trigger cylindrical amphiphiles change their topology to a wedge. The high mobility of the molecules allows for the concentration of the wedge-shaped amphiphiles and the generation of local spontaneous curvature.

A large number of works have dealt with shape transformations driven by curvature changes, but only a much scarce number of works have tackled the effect of molecular topology in the modulation of m_{eff} and shape transformations.[46, 50, 64, 65] Reshaping from spheres to prolates was observed by the trans-cis isomerization during the irradiation of liposomes formed by 100% phosphatidylcholine in which one of the alkyl chains was linked by an azobenzene.[50] The authors demonstrated that the topology change affected the packing of the hydrophobic tails and concomitantly reduced the bending rigidity allowing the shape to evolve. Tube formation was only observed upon external pulling of the membrane. *In situ* ligation of alkyl chains in synthetic lipids allowed the growth of the membrane as well as changes in curvature that were evidenced by the formation of small prolates[46-48].

A different approach to shape transformation inspired by the natural process of apoptosis was proposed by the enzymatic cleavage of cylindrical sphingomyelin into wedge-shaped ceramide. They proved the vectorial nature of the budding and that only 10% of the total lipids were sufficient to induce the formation of multiple buds across the surface.[64] Remarkably, they utilized a similar ratio of ceramide as observed during cell death. These works demonstrated that the topology of the amphiphile can exert some changes in the shape. However, theoretical models predict much more pronounced changes in shape and morphology with m than those achieved so far. Are these changes not achievable by the *in situ* change in the topology of the amphiphiles?

Herein we developed a vesicle system to probe the effect of the *in situ* changes of the topology of an amphiphile on the evolution of shapes for different types of vesicles. The vesicles were self-assembled from two amphiphiles that by virtue of having the same hydrophobic and similar hydrophilic parts homogeneously mixed at any ratio within the bilayers. One of the amphiphiles is stable under UV-Vis irradiation while the other cleaves resulting in the release of the hydrophilic group from the vesicle generating a weak amphiphile with a pronounced wedge shape. This wedge no longer perfectly fits in the bilayer generating an imbalance of forces across the membrane that creates a torque (Fig. 1). The coupling of the molecular interactions results in the membrane's tendency to bend generating non-zero m, which is the driving force for shape transformation (Fig. 1). To perform this study we selected synthetic amphiphiles called Janus dendrimers (JD) that in water self-assemble into vesicles, named dendrimersomes (DSs).[66-70] Although these molecules do not exist in nature, they can be tailored to self-assemble into vesicles that closely mimic

the most important physical properties of cell membranes such as thickness, flexibility, stability, and lateral mobility.[69] They provide a synthetic analog to lipids that is able to co-assemble with the components of human and bacterial cells to form cell-like hybrids, and to mimic natural process such as endocytosis of bacteria.[61, 66, 71] In this study, we assembled the DSs from a photo-stable JD (JD[ps]) and a photo-active JD (JD[pa]) that contain a photo-labile bond that upon cleavage generates a wedge-shaped JD[pa] (w-JD[pa]).[72] DSs with different lamellarities, unilamellar, multilamellar, and smectic-ordered, were prepared in a broad range of JD[pa] ratios and exposed to UV-Vis irradiation while monitoring their shape using confocal laser scanning microscopy (CLSM). Compared to previous studies on GUVs[46-48, 50, 64, 65] it was possible to observe much more complex shape transformations than budding, including tubulation, tube-to-necklace transition, division, generation of daughter vesicles, and formation of high genus vesicles allowing to probe a much broader morphology space as a function of molecular topology. But how relevant are these shape transformation to cells? For decades it had been accepted that the characteristic shape transformations via flickering of red blood cells reflected an instability of a living system under non-equilibrium conditions.[73, 74] Thus, flickering was related to an active process.[66, 67] But actually, it was much simpler. The essential property of bilayers is that they optimize their shape at a fixed number of amphiphilic molecules.[75] Brochard-Wyart showed that flickering in red blood cells could be understood from a model containing only curvature energies plus viscous forces and this was one of the starting points for many studies on bilayers, pioneered by Helfrich.[76] Several of the examples shown in this work resemble cellular processes observed in living cells and may help to elucidate some functions of living matter.
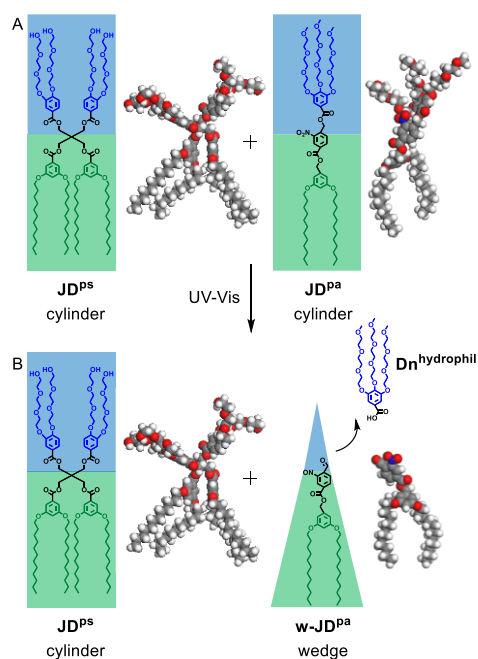
Fig. 2. Chemical structures and quantum mechanical geometry optimization of photo-stable JD (JD[ps]) and photo-active JD (JD[pa]) before (A) and after irradiation (B) with UV-Vis light.

## Results and Discussion

Janus dendrimers

Two amphiphilic JDs were designed and synthesized to have a packing parameter close to one resembling a cylindrical shape so that the vesicular morphology is the preferred lyotropic phase.[77] Both dendrimers have the same hydrophobic dendron and a similar hydrophilic one to prevent phase segregation during co-assembly. The hydrophobic 3,5-didodecyloxyl benzoic dendron was synthesized via a direct etherification of 3,5-dihydroxybenzoate with 1-bromododecane.[69] The photo-stable twin-twin JD[ps] was synthesized by connecting the hydrophilic hydroxy terminated 3,4-bis-tri(ethylene oxide) benzoic dendron to the hydrophobic dendron via a pentaerythritol core.[69] In case of the photo-active single-single JD[pa] the hydrophilic methoxy terminated 3,4,5-tris-tri(ethylene oxide) benzoic dendron is linked to the hydrophobic dendron via a photocleavable *o*-nitrobenzyl (NB) group.[72, 78, 79]

We analyzed the photolytic cleavage of the NB group resulting in the formation of two fragments by High Resolution Electrospray Ionization Mass Spectrometry (HRESI-MS). During the irradiation of a JD[pa] solution in acetonitrile with UV-Vis light (λ = 405 nm), the NB group was cleaved leading to the precipitation of the weakly amphiphilic minidendron (w-JD[pa]) that contains the hydrophobic dendron linked to an aldehyde group. The other fragment of the molecule, containing the hydrophilic dendron with an acid moiety (Dn[hydrophil]) remained in solution and was analyzed by HRESI-MS confirming the previously reported cleavage (Fig. S 1).[72]

The topology of the amphiphile dictates its packing parameter and ultimately the *m*.[77] We assessed how the cleavage of JD[pa] changes the molecular shape by conducting a semiempirical conformational analysis. The geometry of a single molecule in water was optimized by a quantum mechanical calculation applying the permittivity of water as a continuum. This model provides a simplified approximation to the JD geometry. The simulations confirmed a cylindrical shape of JD[pa] and JD[ps] before irradiation (Fig. 2 A). However, after the cleavage of the photolabile NB bond in JD[pa] (Fig. 2 B) the shape of the weakly amphiphilic minidendron resembles a wedge (w-JD[pa]). The new shape imposes spontaneous curvature leading to various shape transformations in the DS membrane. We assessed the effect of the concentration of w-JD[pa] on the shape transformation by varying the molar ratio of JD[pa] co-assembled with JD[ps]. DSs were assembled with different compositions ranging from 1 to 100 mol% JD[pa], *i.e.* DS-1, DS-10, DS-40, DS-70, and DS-100. Co-assembled DSs were characterized via optical microscopy, cryo-FESEM, and cryo-TEM. Real-time visualization of shape transformations was performed in CLSM.

Self-assembly into vesicles

DSs were formed by the self-assembly of dendrimers at different ratios using thin-film hydration or the injection method. The former method gives access to giant vesicles while the latter results in small vesicles that are advantageous for cryo-TEM imaging. The kinetically controlled nature of the assembly processes in both methods yields vesicles with different lamellarity including uni- and multilamellar vesicle types but with membranes with the same thickness (5.1 nm, as demonstrated by cryo-TEM and wide angle X-ray scattering, Fig. S 2).[29, 68]

Bright-field	Polarized	CLSM	Cryo-FESEM	Cryo-TEM
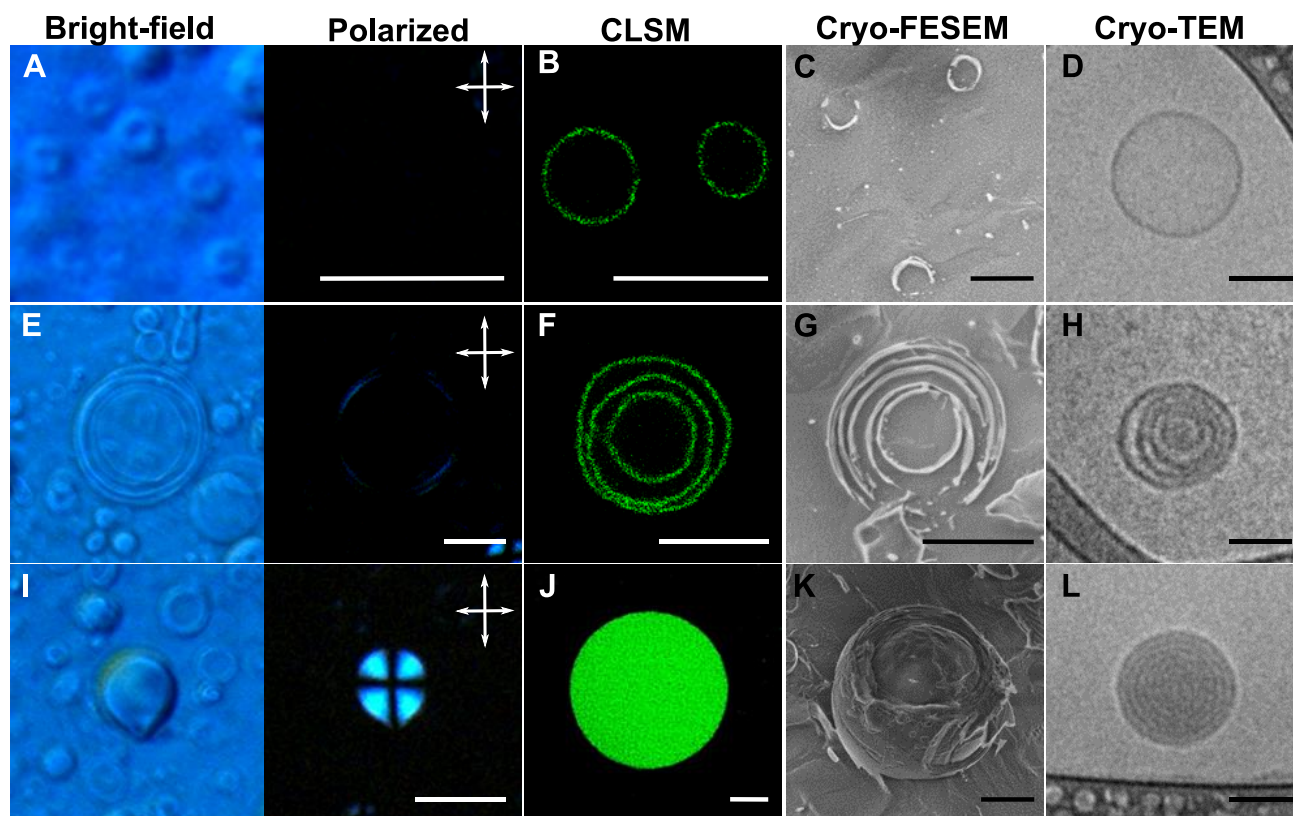
Fig. 3. Types of DSs vesicles. Optical microscopy, confocal laser scanning microscopy (CLSM), cryogenic field emission scanning ele ctron microscopy (cryo-FESEM), and cryogenic transmission electron microscopy (cryo-TEM) were utilized to characterize unilamellar (A-D), multilamellar (E-H) and smectic-ordered vesicles (I-L). Vesicles were prepared by thin-film hydration method for optical, CLSM, and cryo-FESEM characterization and by injection method for cryo-TEM characterization. In optical microscopy, vesicles were imaged in bright field (left side) and polarized mode (right side). BODIPY fluorophore was utilized in visualization by CLSM. Scale bars are 20 μm (optical microscopy: A, E, J), 10 μm (CLSM: B, F, J), 5 μm (cryo-FESEM: C, G, K) and 50 nm (cryo-TEM: D, H, L).

In the injection method, a solution of dendrimers in a water-miscible organic solvent is added into water. The almost instantaneous mixing of the solvents results in a spinodal-like decomposition of nanoaggregates that grow in a diffusion-controlled manner into discs and subsequently into vesicles.[80-82] The JDs in the aggregates arrange into small vesicles of relatively homogeneous size.[67, 70] On the other hand, during rehydration of thin JD films, the preorganized JD bilayers undergo swelling starting from the bilayer in direct contact to water. To maximize the contact of the hydrophilic dendrons with the water phase JD bilayers detach from a Teflon surface. Due to the hydrophobic effect and a high edge tension at the exposed bilayer edges the bilayer fragments bend and close into vesicular assemblies.[29, 82] Thus, the thin-film hydration method gives rise to larger vesicles with a broader size distribution.

Within vesicles with different lamellarity, multilamellar vesicles are the thermodynamically most stable type representing the lowest free energy vesicle morphology. Upon dissipation of energy into the system higher energy structures such as unilamellar morphologies are obtained.[82, 83] Figure 3 shows DSs self-assembled via both techniques which yielded mainly unilamellar, multilamellar, and smectic-ordered vesicle types.

Unilamellar vesicles (Fig. 3 A—D) displayed a preferential spherical shape in bright field (BF) obtained from optical microscopy. In the polarized (Pol) mode no birefringence could be observed. CLSM, cryo-FESEM, and cryo-TEM confirmed spherical structures with one bilayer and a vesicle lumen. A

second type of DS morphology was observed in which multiple individual concentric bilayers could be distinguished in BF optical microscopy (Fig. 3 E—H). Very weak birefringence was observed in the Pol mode suggesting no registry between the bilayers. Imaging the cross-sectional area of the vesicle in CLSM, cryo-FESEM, or cryo-TEM confirmed that the bilayers were separated (Fig. 3 F—H) proving that this morphology corresponded to multilamellar vesicles. A third type of DS was observed as spherical full objects with indistinguishable bilayers in BF and CSLM (Fig. 3 I—L) while a distinct Maltese cross could be observed in the Pol microscope. This observation indicates multiple bilayers (L_α) with registry. This lyotropic phase is the equivalent to the thermotropic smectic mesophases.[84] These smectic-ordered DSs are a type of multilamellar vesicles where the lamellae are packed close to each other to form smectic-ordered liquid crystals. Fig. 3 K shows a cryogenically fractured giant DSs displaying concentrically closely packed bilayers. The smectic nature was further confirmed by cryo-TEM (Fig. 3 L). The smectic arrangement might be mediated by strong interbilayer hydrophilic interactions.

In the following sections, we analyzed the shape transformations and studied their mechanism by focusing on each type of vesicle separately. All morphological transformations are discussed as a function of irradiation time and concentration of JD[pa].
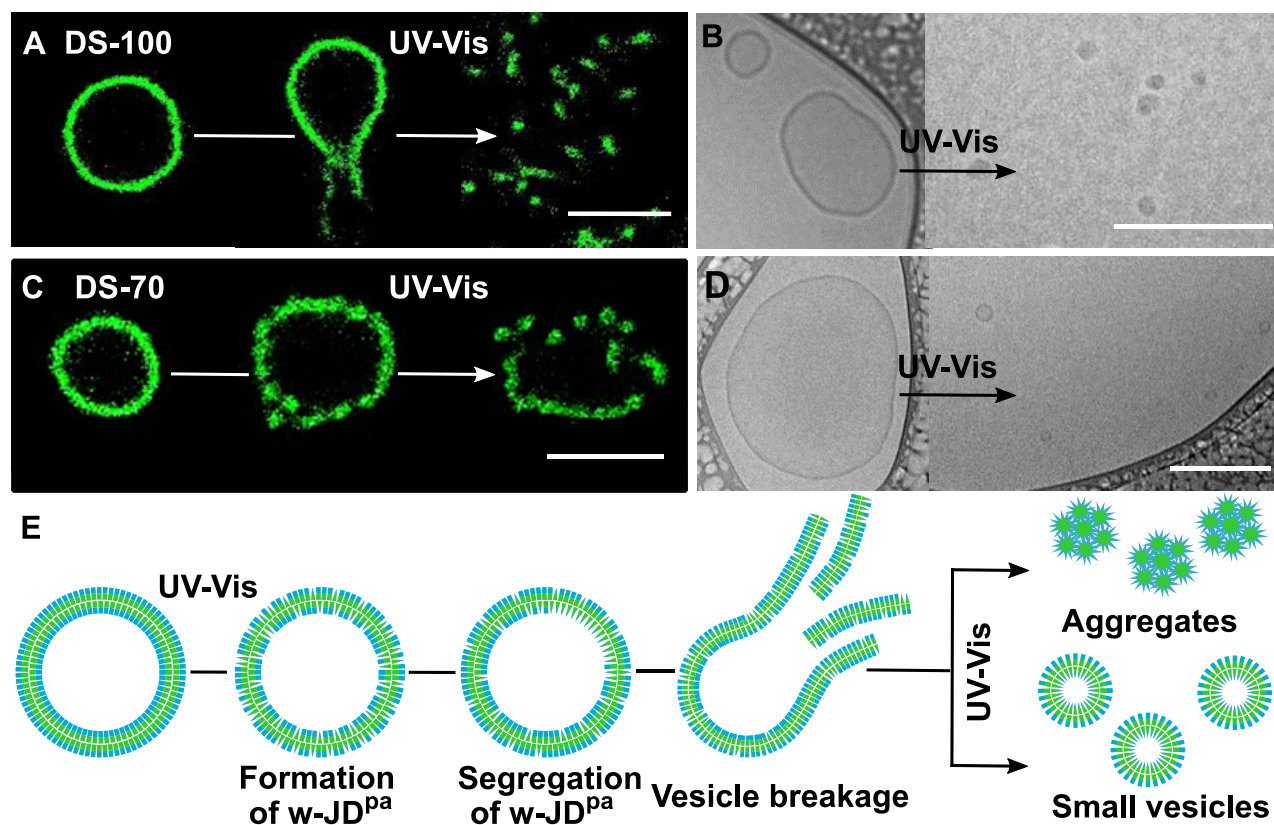
Fig. 4. Shape transformation of unilamellar vesicles with a high content of JD^{pa} upon irradiation with an UV-Vis laser. CLSM images (A) and cryo-TEM (B) showing the process of disassembly of vesicles into globular aggregates upon UV-Vis irradiation. CLSM (C) and cryo-TEM (D) images reveal that with the addition of 30% of JD^{ps} (DS-30) disassembly of vesicles upon irradiation leads to the formation of new small vesicles. (E) Schematic representation of the morphological transformation of unilamellar DSs with a high content of JD^{pa}. The proposed mechanism includes changing the topology of cylindrical JD^{pa} into wedge-shaped JD^{pa} (w-JD^{pa}), their lateral segregation, and disassembly into either globular aggregates (DS-100) or small vesicles (co-assembly of JD^{pa} with JD^{ps}). Scale bars are 5 μm (CLSM: A and C) and 200 nm (cryo-TEM: B and D). Background in CLSM is cropped.

Unilamellar DSs

The genesis of different shapes was directly monitored by CSLM while irradiating with UV-Vis light (λ = 405 nm). We studied DSs whose radii were much larger than the bilayer thickness and having an initial spherical shape, which is a minimal surface. Irradiation of the DSs cleaved the NB bond, part of the JD^{pa} core, resulting in the formation of an acid-containing hydrophilic fragment Dn^{hydrophil} and a minidendron, w-JD^{pa}, with an aldehyde moiety.[72] The cleavage invariably led to pronounced effects on the shape of the DSs for all ratios of JD^{pa} while no shape changes where observed for DS-0 or without irradiation (Fig. S 17 and S 18 in the ESI). This observation indicates that JD^{pa} was not only cleaved but that the w-JD^{pa} fragment remained as part of the membrane. This fragment has a much smaller hydrophilic area; thus, the total area of the membrane has to shrink. For spherical vesicles, a decrease in the total area must be accompanied by a decrease in the volume of the vesicle which causes a change in the reduced volume ($v = 6\sqrt{\pi}\,\frac{V}{A^{3/2}}$), defined as the ratio of the vesicle's volume V to the volume of a sphere with the same surface area A.[41] Furthermore, the wedge shape of w-JD^{pa} imposes transmembrane asymmetries which drive membrane bending.[34, 35, 38, 42, 85] These asymmetries include a local term (m), and a non-local (m_{nlo}), which combine into m_{eff}. Thus, m_{nlo} and v are the most relevant parameters dictating the stationary thermodynamic morphologies.[33] We

hypothesized that the dynamics and extent of these effects can be controlled by the concentration and the mobility of w-JD^{pa}. Thus, we assessed the shape transformation for individual vesicles with different concentrations of JD^{pa}.

Irradiation of DS-100 vesicles (Fig. 4 A) resulted in membrane undulations followed by almost immediate disassembly. Presumably, the simultaneous formation of a large number of w-JD^{pa} led to instability allowing fission and disintegration of the membrane into aggregates composed of the cleaved hydrophobic minidendron. The disassembly process was directly monitored by CSLM (video S 1) showing that the hydrophobic BODIPY remained localized in the aggregates confirming their hydrophobic nature. Cryo-TEM revealed the generation of globular aggregates with a uniform contrast indicating the homogeneous composition of their interior (Fig. 4 B and Fig. S 3). We propose a mechanism for the formation of the aggregates as depicted in Fig. 4 E. Irradiation generates a large number of w-JD^{pa} homogeneously distributed across the whole bilayer. The wedges do not match the packing parameter for the assembly into a bilayer creating instabilities. During the initial stages of irradiation, more and more wedges are generated leading to a decrease in total membrane area which concomitantly increases the inner pressure to expel water from the inside to reduce the volume.[35, 86-88] The abrupt increase in pressure caused the burst of the membrane (Fig. 4 A). Further irradiation generates even more wedges that

do not fit into a bilayer assembly. In the case of 100% JD^{pa} all molecules are cleaved into w-JD^{pa} whose packing parameter is incompatible with bilayer structures, thus the hydrophobic effect forces their assembly into small hydrophobic aggregates. Decreasing the ratio of JD^{pa} to 70% (DS-70) (Fig. 4 C) resulted in a different disassembly process. Instead of an abrupt burst and complete disintegration, the irradiation induced membrane undulations (Fig. S 10–S 11) followed by the simultaneous fission of the membrane into smaller membrane fragments of approximately the same area that closed into smaller vesicles. Cryo-TEM confirmed the formation of the smaller DS vesicles as the product of irradiation (Fig. 4 D). The generation of daughter vesicles with approximately the same size requires the fast diffusion and formation of JD^{ps} domains surrounded by w-JD^{pa} prior to the fission of the membrane as described by Gozdz.[89] The phase separation between JD^{ps} and w-JD^{pa} is driven by their shape mismatch while fission is a consequence of line tension between the domains and the failure of w-JD^{pa} to form stable bilayers as demonstrated for DS-100. Such a mechanism can only be feasible if JD^{ps} can diffuse faster than fission occurs, which demands a high lateral mobility of the amphiphiles. The fluidity of the membrane was assessed by determining the diffusion coefficient of a hydrophobic dye (BODIPY) in the membrane by fluorescence recovery after photobleaching (FRAP). Vesicles containing BODIPY embedded in the hydrophobic domain of the bilayer membrane were bleached by an Ar$^+$ laser. After analyzing the fluorescence recovery time, a diffusion coefficient of $0.67 \pm 0.25 \ \mu m^2 \cdot s^{-1}$ was calculated which closely resembles the mobility of lipids in plasma membranes ($1 \ \mu m^2 \cdot s^{-1}$).[90, 91] It is worth noting that the observed diffusion coefficient is about two orders of magnitude higher than for polymersomes ($2.4 \cdot 10^{-3} \ \mu m^2 \cdot s^{-1}$)[92] assembled from amphiphilic block copolymers. This highlights the biomimetic nature of the DSs. Such fast lateral mobility results in diffusion faster than the time required for membrane rupture (20—30 s) supporting the proposed mechanism.

Unilamellar vesicles with a reduced content of JD^{pa} follow a different shape transformation pathway, depicted in Fig. 5. From the videos S 2–S 3 (DS-40 and DS-10) it was evident that irradiation generally resulted in an increase of membrane undulations (Fig. S 10–S 11) indicating a reduction of tension by the release of water from the vesicle lumen. Such transient pores are formed when the internal pressure is higher than 2σ (the interfacial tension). The pores allow the content of the vesicle to exit, the tension to drop and the pore to stop growing. Subsequently the pore closes due to the line tension.[35, 86-88, 93] DSs with 10–40% JD^{pa} (Fig. 5 A–C) underwent a budding process followed by an elongation into tubular structures, that subsequently evolved by tube-to-necklace transitions into beads connected by necks. The bead formation started at the distal end of the tube and continued inwardly where all beads formed with the same size as theoretically predicted.[56, 94, 95] In DS-40 (Fig. 5 A) multiple buds formed simultaneously and evolved into separated tubes that morphed into necklaces. Further irradiation led to the fission of the membrane at the level of the neck and the release of independent vesicles of roughly the same size. Decreasing the content of JD^{pa} to 10% (DS-10) resulted in a similar shape evolution but depended on the initial size of the mother DS vesicle. In DSs with a smaller diameter a single tube was formed which led to a string of beaded vesicles (Fig. 5 B). Increasing the diameter of the mother vesicle resulted in the simultaneous formation of multiple buds of similar size which grew into tubes. In a subsequent step, the tubes underwent beading that resulted in a morphology resembling a starfish (Fig. 5 C). Lowering the content of JD^{pa} even further (DS-1) resulted in a gradual change in shape starting from the prolate vesicle, followed by an asymmetric dumbbell consisting of two spheres, a large and a small one. Further irradiation led to multispherical morphologies, consisting of a chain of small spheres connected by stable closed necks. Fig. 5 D depicts the formation of a chain of five spheres.

Budding followed a similar route as for the DSs with higher JD^{pa} discussed above. Irradiation also generated wedges, however, the lower content was not sufficient to induce fission for DS-10 and DS-1 and only at later stages in DS-40. Irradiation was accompanied by fluctuations consisting of the superposition of various oscillatory modes (Fig. S 11). Increasing the content of JD^{pa} increased the fluctuation of a shorter period supporting that the generation of w-JD^{pa} and the intermolecular coupling of motion[63] were the driving force for shape transformation. The rapid lateral mobility of w-JD^{pa} can allow segregation and local asymmetries in the membranes, *i.e.* local non-zero m. If a section of the membrane has a higher density of w-JD^{pa} in the external leaflet a torque will be generated aiming at forcing the membrane to achieve a negative curvature (local negative m). Conversely, if the density of w-JD^{pa} is higher in the internal leaflet the torque aims at achieving a positive curvature (local positive m). The formation of a bud requires negative curvature in the zone of the neck and positive curvature on the dome (Fig. 1). The observed transitions in Fig. 5 require that during irradiation the DSs moved diagonally in the morphology diagram, *i.e.* simultaneously reducing their v while increasing m_{eff}.[96, 97] Since all budding processes observed here are outward-directed, we can conclude that the irradiation led to m_{eff} greater than zero. But by which mechanism can m_{eff} be greater than zero when w-JD^{pa} is generated at the same rate in the inner and outer leaflet?

As alluded before, photocleavage invariably leads to a reduction of area of the membrane and a concomitant increase in pressure, which is released by an outward flow of water allowed by the formation of transient pores as described by Helfrich and Brochard-Wyart.[86-88, 98] Such a flow of water through the membrane produces a parallel transport of amphiphiles along the pressure gradient in spite of the concentration gradient, ultimately leading to an increase of the A^{out} [35, 86, 99] at the expense of shrinking A^{in}, thus generating a positive m_{nlo}. If flip-flop is not allowed, the non-local term dominates and out-budding occurs.[35] On the other hand, if flip-flop is allowed, w-JD^{pa} can preferentially be translocated to the internal leaflet generating a positive m. Such a flip-flop mechanism is observed for cholesterol in liposomes. Cholesterol and w-JD^{pa} are structurally similar, both having a small hydrophilic head group and a large hydrophobic tecton; thus, their flip-flop in a time range of the experiment might be feasible.

Fig. 5. Shape transformation of unilamellar vesicles with a reduced content of JD^{pa} upon irradiation with an UV-Vis laser. CLSM images show that UV-Vis irradiation of unilamellar DS-40 (A) and DS-10 (B, C) vesicles led to the formation of tubes followed by beaded vesicles. (D) CLSM images show that irradiation of DS-1 led to the formation of a prolate vesicle, followed by an asymmetric dumbbell, and finally, multispherical morphologies, where five small spheres are connected by stable closed necks. (E) Schematic representation of its mechanism including a change of the topology of cylindrical JD^{pa} into w-JD^{pa}, their lateral segregation, and formation of local spontaneous curvature that leads to tubulation and the formation of beaded vesicles. Scale bars are 10 μm. Background in CLSM is cropped.

When the composition of JD^{pa} was between 10 and 40% (DS-10 and DS-40) the bud grew into a tube. Tubular structures are stable at low values of m_{eff}. Increasing m_{eff} by irradiation induces the beading process. In these conditions, tubular structures are less stable than catenoids (a minimal surface); thus, the cylinder beads from the distal ends passing through unduloids with a different number of beads. The number of beads evolved gradually until all cylinders consisted of chains of spheres of approximately the same size connected by closed necks representing a minimum in the free energy (Fig. 5 A—B, last irradiation time). On the other hand, when the content of JD^{pa} was lower, the transitions began with the formation of a prolate DS that upon further irradiation generated an asymmetric dumbbell and then a chain of beads. At initial irradiation times, there were spheres with two sizes, one large and several small ones. This is well in line with models demonstrating that for any multispherical morphology formed from a homogeneous membrane, the individual spheres either

have two different radii or are all of the same sizes.[100] In our systems evolving from tubular and prolate DSs, the final morphology resulted in spheres of the same size. These observations are a direct proof that all spherical membrane segments are subjected to the same mechanical tension. Interestingly, this type of transformation can be related to the cellular process of programmed cell death —apoptosis. Apoptosis generally involves the formation of highly curved membrane protrusions that undergo tubulation, beading, and further fragmentation processes. It has been suggested that the generation of membrane protrusions involved in apoptosis may be driven by the enzymatic cleavage of sphingomyelin into ceramide with a concomitant change in the topology of the lipid similar to the one presented here.[64] Remarkably, the content of the wedge-shaped lipid (ceramide) in apoptotic cells amounted to 10% which corresponds to the percentage of w-JD^{pa} in DSs that exhibit similar shape transformations. While apoptosis cannot be exclusively linked to changes in the spontaneous curvature of the membrane, recent studies have demonstrated only a small influence of the cytoskeleton in the morphological changes.[64]

The stability of the multispherical shapes is determined by the stability of the closed membrane neck with respect to the open neck. A closed neck is stable when

$$\bar{m}_{eff} = m_{eff} \cdot R_{ve} \geq \frac{R_{ve}}{2}\left(\frac{1}{R_a} + \frac{1}{R_b}\right)$$ [100] with $\bar{m}_{eff}$ as the effective dimensionless spontaneous curvature, R_a and R_b as the radii of the spheres connected by the neck, and R_{ve} as the radius of the initial mother vesicle. The multisphere structures for DS-10 and DS-1 were stable after irradiation, thus we utilized the stability condition to estimate the minimum value of $\bar{m}_{eff}$ for each system. A $\bar{m}_{eff}$ of at least 3.9 was necessary for the DS-1 to achieve stable conditions while $\bar{m}_{eff}$ larger than 10.9 was necessary for DS-40 (Fig. S 15). Thus, a higher content of JD^{pa} results in a higher effective spontaneous curvature after irradiation, as it is expected.

Multilamellar DSs

We analyzed a large number of multilamellar vesicles as a function of irradiation time and the molar ratio of JD^{pa}. The irradiation of the membrane induced undulations followed by the formation of double bilayers which are connected by a lattice of passages. These types of morphologies are known as high genus structures with membrane-linking pores (MLPs).[94, 101-103] All DSs studied had a genus on the order of $g \approx 100$. DSs co-assembled from a low density of JD^{pa} (1%–20%) generally followed the same characteristic morphological transformation resulting in spheres with large pores. CLSM and cryo-FESEM of DS-1 vesicles after irradiation showed a spherical high genus vesicle with pores organized in a hexagonal lattice (Fig. 6 B–C and video S 4). Furthermore, a Z-scan gave access to the three-dimensional internal arrangement of membranes and pores (Fig. 6 A). It revealed a spherical structure where the bilayer membranes of the internal and external vesicles are connected by multiple pores. Such a type of arrangement is termed nucleus-type MLP vesicle.[102] Increasing the density of JD^{pa} (30%–70%) led to the formation of slightly different high genus morphologies. The evolution of the shape of a multilamellar (two lamellae) DS could be observed in real-time by CSLM (Fig. 6 E for DS-30, videos S 5 and S 6 for DS-30 and video S 7 for DS-70). The irradiation induced undulations and the simultaneous morphing of the internal and external bilayers

into a prolate shape which then generated an asymmetric dumbbell. Thus, the initial steps of shape transformation corresponded to the ones observed for unilamellar vesicles as a consequence of increasing the m. The undulations were more pronounced when the content of JD^{pa} was higher. These rapid movements enabled multiple contacts between the bilayer membranes which were directly followed by pore formation.[104-106] Cleavage of the two apposing bilayers occurred simultaneously at the neck of the initial prolate vesicle, releasing a two-dimensional disk-like structure (Fig. 6 E–F). Due to their flat nature and the formation of multiple organized pores, such structures are termed honeycomb-type MLP vesicles.[102] Honeycomb-type MLP DSs are formed when two apposing bilayers fuse at a large number of points simultaneously.[103, 107-109] Cryo-FESEM confirmed the highly ordered flat structures as the product of irradiation (DS-30, Fig. 6 G). Similar high genus structures play an important role in various transport mechanisms in nature and are highly interesting systems due to their ability to open and close their pores in response to small external changes.[94, 110] An important example is the unique high genus structure of the nuclear envelope of cells which is responsible for the transport between the nucleus and cytoplasm.[111] In cells, the formation of a high genus topology is mediated by the fusion of lipid membranes followed by an assembly of a variety of curvature-sensing proteins forming the nuclear pore complex (NPC) that stabilizes the large pores.[112] But how can such large pores form in multilamellar DSs?

The formation of pores requires that the membranes first approach, locally arrest their undulations, adhere, and then fuse generating large pores. Approach and adhesion require attractive interactions, which are in general prohibited by the hydration repulsion of the hydrophilic groups on the periphery of the vesicles.[113-115] In liposomes, such localized adhesion is driven by hydrophobic point defects in which hydrophobic groups are transiently exposed to water promoting the interbilayer adhesion.[105, 115, 116] No pore formation was observed for any multilamellar DSs before irradiation, indicating that the hydrophilic dendrons exerted an effective repulsive potential (Fig. 3 E—H). However, irradiation rapidly enabled the formation of adhesive contacts (Fig. 6). The photocleavage of JD^{pa} releases the hydrophilic dendron (Fig. 2), resulting in a local reduction of the hydrophilic repulsion and allowing critically close apposition of the interacting membranes and the establishment of hydrophobic interactions that mediate adhesion (second step in Fig. 6 E). Cullis and Siegel developed a theory for the fusion of lipid bilayers and the generation of pores based on the formation of non-bilayer structures at the contact point.[108, 109, 117-119] The theory describes the formation of a short-lived inverted micellar intermediate (IMI) followed by a long-lived metastable structure termed interlamellar attachment (ILA, Fig. 6). This transition requires that the IMI fuses with the surrounding monolayers to form an ILA that is a fusion channel between two bilayers. In our DSs, interbilayer adhesion is driven by the presence of w-JD^{pa}, thus the adhesion zone concentrates these amphiphiles which have a packing parameter commensurate with the formation of inverse micelles. Thus, it is feasible that the adhesion events led to the organization of w-JD^{pa} into an IMI as proposed by Siegel which rapidly evolved into a pore.
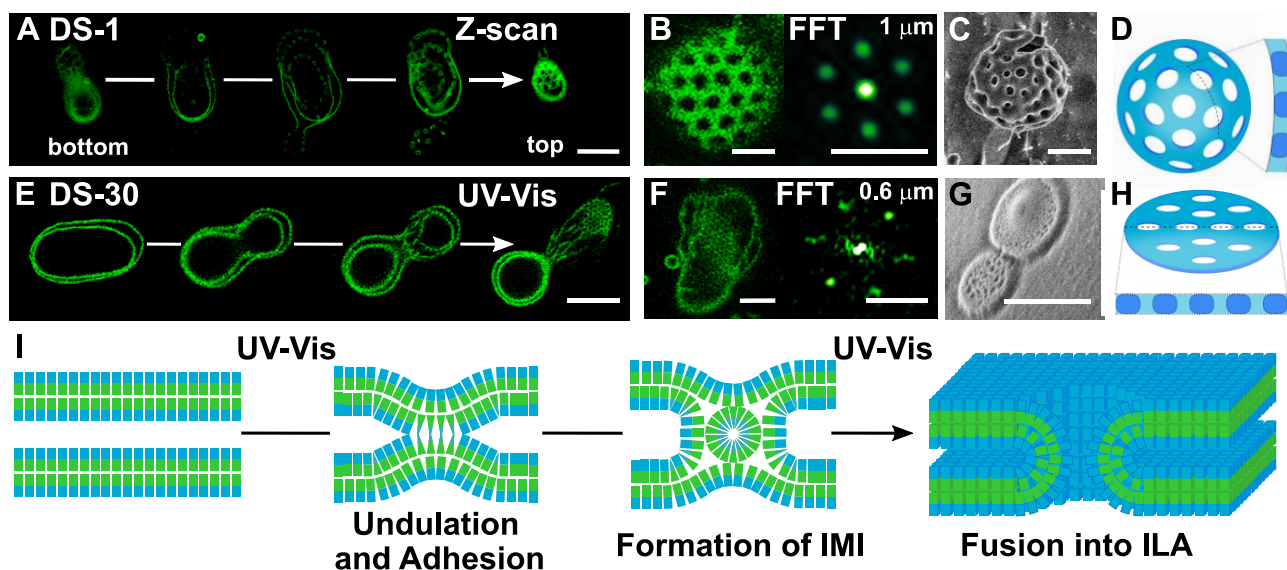
Fig. 6. Microscopic images of vesicles with membrane-linking pores (MLPs). (A) CLSM Z-scan of a stable nucleus-type MLP DS formed after UV-Vis irradiation of a multilamellar DS-1 vesicle (Scale bar is 10 µm) and (B) the FFT analysis of a nucleus-type MLP DSs formed from multilamellar DS-10 vesicles (Scale bars are 5 µm^{-1} and 2 µm^{-1}); the lattice parameter of the pore array is 1 µm. (C) An example of a nucleus-type MLP DS observed by cryo-FESEM (Scale bar is 2 µm) and the schematic representation (D). (E) CLSM images showing the formation of honeycomb MLPs by irradiation of multilamellar DS-30 (Scale bar is 10 µm) and its FFT analysis; the lattice parameter of the pore array is 0.6 µm (F) (Scale bars are 5 µm^{-1} and 2 µm^{-1}). (G) An example of honeycomb-type MLP DSs observed by cryo-FESEM (Scale bar is 1 µm) with the schematic representation (H). (I) MLP formation mechanism induced by a change of the topology of JD^{pa} via UV-Vis irradiation. Background in CLSM is cropped.

Both types of structures, nucleus-type and honeycomb-type MLP DSs, displayed large circular pores, compared to the interbilayer separation with a narrow distribution of radii (Fig. 6 and Fig. S 12). This finding agrees with previous theoretical considerations showing that large passages were favored for larger m. The pores were organized into nearly perfect hexagonal arrays with lattice parameters of the pore array ranging from 0.6—1 µm as demonstrated by the fast Fourier transform (FFT) of confocal images (Fig. 6 B and F). This arrangement of pores minimizes the tension between pores which is caused by an abrupt inversion of curvature.[94, 101, 111, 120, 121] Furthermore, we found that the lattice parameter decreased with an increasing ratio of JD^{pa} (Fig. S 13). Analogously, the radii of the pores decreased with an increasing ratio of JD^{pa} from 450 to 150 nm for DS-1 to DS-40 and remained constant thereafter (Fig. S 12).

Smectic-ordered DSs

Smectic-ordered DSs with a JD^{pa} content between 10—100% were irradiated at the equatorial plane while their shape transformation was monitored in CLSM (video S 8). The irradiation area is a spherical segment at the equatorial level with 500 nm in height. The evolution of the structure followed the same pathway for all studied compositions (Fig 7 and Fig. S 5–S 8). Fig. 7 A depicts the transformation of a spherical smectic vesicle with a molar ratio of 40% JD^{pa} (video S 8). The first step comprised the generation of small outward-pointing buds at multiple points around the whole external circumference almost immediately upon the commencement of irradiation. A three-dimensional Z-Scan from the bottom to the top of the DS-100 at a similar stage of transformation revealed that the formation of daughter buds was not restricted to the irradiated spherical segments but formed all over the surface of the DSs (Fig. 7 B). For a given DS composition the out-buds had approximately the same size and grew into spherical structures

in close proximity to each other. After reaching a certain bud size, a stable closed neck formed at the contact point of the spherical bud and the mother DS. After further irradiation, the necks were severed resulting in daughter vesicles (Fig. 7 A, last stage). Most daughter DSs remained weakly associated with the mother DSs. We define the outermost coat of daughter vesicles as daughter vesicles of the first generation (G1). With increasing irradiation time, the second generation (G2) of daughter vesicles emerged between the periphery of the mother vesicle and the previously formed generation of daughter vesicles. Remarkably, the daughter DSs displayed a narrow size distribution for a given composition, suggesting that the density of JD^{pa} governed the formation of the daughter vesicles (Fig. S 14).

We propose a general mechanism combining features of the mechanisms observed for unilamellar and multilamellar DSs to account for the homogeneous generation of daughter vesicles across the whole surface of the mother DSs. Irradiation at the spherical segment generated w-JD^{pa} in all leaflets of the tightly packed bilayers. This is a non-bilayer-forming amphiphile that generates larger m and hydrophobic point defects, which are the driving force for shape transformation. Buds of approximately the same size formed across the whole surface simultaneously (Z-scan in Fig. 7 B) and not only in the irradiated zone. On the one hand, this requires that apposing bilayers must have fused to provide sufficient area to cover the entire mother DS periphery with buds which then closed and shed daughter DSs.[105] On the other hand, it also proves that the diffusion of w-JD^{pa} (in the order of µm^2·s^{-1}) was faster than the process of shape transformation observed here (tens of seconds).
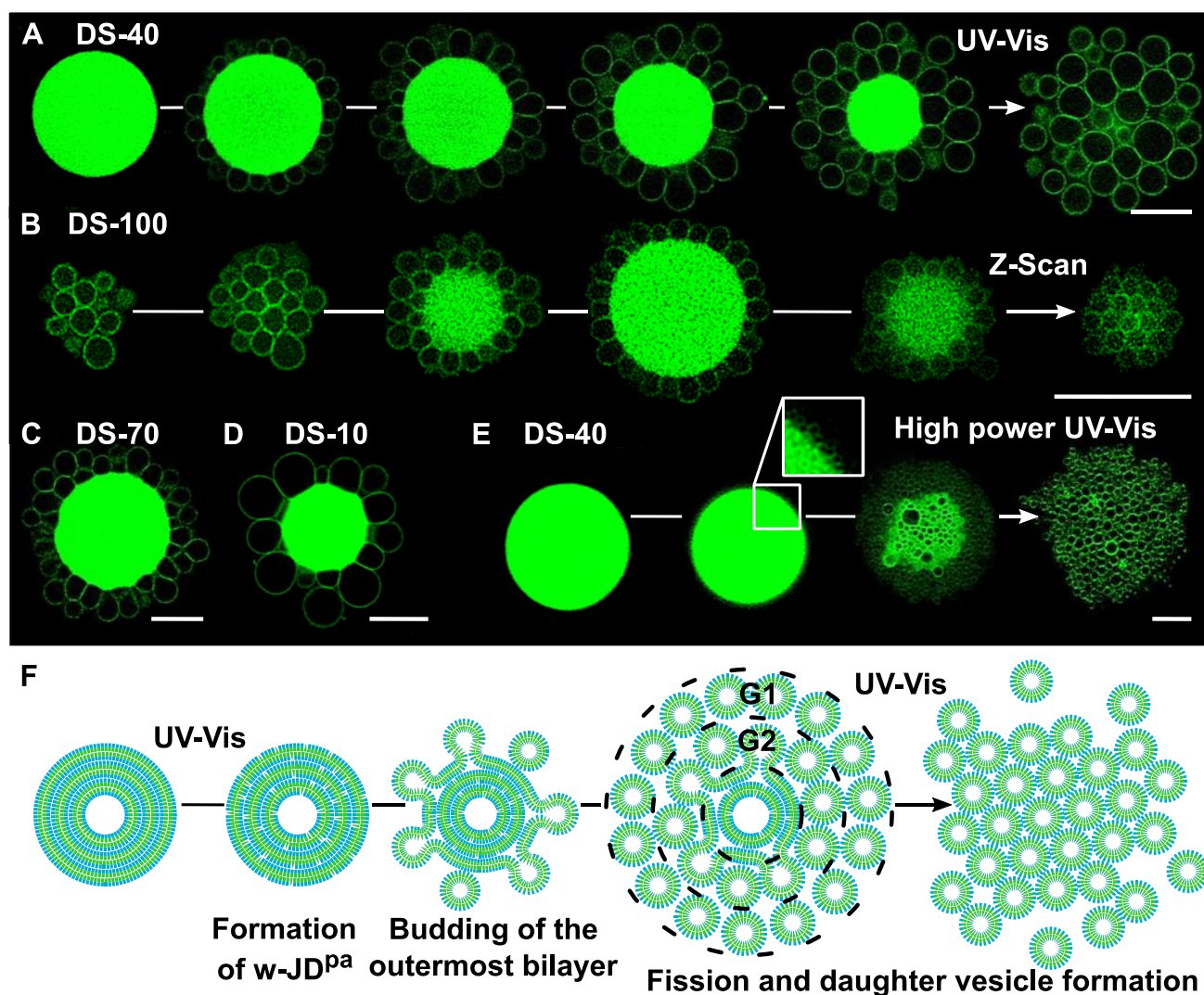
Fig. 7. Shape transformation of smectic-ordered vesicles. (A) CLSM image sequence showing the formation of small daughter vesicles from a smectic DS that contained 40% JDpa upon UV-VIS irradiation. (B) CLSM Z-scan of a smectic vesicle (100% JDpa) after short-time irradiation with UV-Vis in the confocal plane located in the equatorial plane of the DS. Buds formed across the whole area of the DS. The size of the daughter vesicles is controlled either by the concentration of JDpa (C and D) or by the intensity of the UV-Vis laser (E). (F) The mechanism of shape transformation of smectic vesicles includes a change in the topology from cylindrical JDpa into w-JDpa, their lateral segregation, relaxation of the outermost bilayer by budding that culminates in fission and the release of new daughter vesicles. Background in CLSM is cropped.

We hypothesize that these w-JDpa could generate hydrophobic point defects which mediated interbilayer adhesion and fusion, favored by the perfect apposition of the bilayers in a similar fashion as observed for multilamellar DSs (*vide supra*). This is in agreement with the observation of the same mechanism for DS-100 to DS-10. In this mechanism, the size of the vesicle is the result of the competition between diffusion and generation of local m. This is evidenced by the inverse relationship between the size distribution of daughter DSs and the ratio of JDpa before irradiation. Statistical analysis of the size distribution of the daughter DSs indicates that their size increased with decreasing ratio of JDpa. The distributions were normal with low kurtosis and skewness (Fig. S 14). The minimum dimensionless spontaneous curvature $\overline{m}_{eff}$ was calculated from the stability conditions for a closed neck (*vide supra*). We obtained a minimum value of $\overline{m}_{eff} \geq 2.09$ for DS-10 which monotonically increased with the ratio of JDpa until $\overline{m}_{eff} \geq 3.37$ for DS-100 (Fig. S 16). A 4-fold increase in the laser power resulted in the formation of a very large number of small out-buds only at the

spherical segment that was irradiated (Fig. 7 E, inset). Moreover, further irradiation led to the formation of cavities even inside the DS-40. This indicates that the faster rate of formation of w-JDpa with a high laser power must have exceeded the ability of JDpa to diffuse, thereby accumulating the wedge-shaped amphiphiles in a small area leading to a higher local m and a concomitant more pronounced shape transformation restricted mainly to the irradiated volume.

Conclusions

In this work, we systematically dissected the effects of the *in situ* change of the JD topology on the morphology of DS membranes for different vesicle types and ratios of w-JDpa. We elucidated the different pathways for shape transformation. Irradiation of unilamellar DS-100 and DS-70 resulted in undulations across the whole membrane followed by fission. DS-100 disassembled into small hydrophobic aggregates while

in the case of DS-70 the membrane was severed into smaller fractions that closed into small daughter DSs with a narrow size distribution. The latter required the fast diffusion and formation of JD^{ps} domains surrounded by w-JD^{pa} prior to the fission of the membrane. Fission might be the result of line tension between the two domains.

Shape transformation began with outward-directed budding for the other unilamellar DSs with a lower ratio of JD^{pa}. DS-40 and DS-10 underwent rapid budding followed by the formation of tubular structures that evolved by the tube-to-necklace transition into spherical beads connected by closed necks. Lowering the content further (DS-1) resulted in a different pathway including the formation of prolates and asymmetric dumbbells, which culminated in multispherical morphologies. These shape transformations required a simultaneous decrease in ν and an increase in m_{eff}. Using the stability condition for a closed neck we proved that the minimum m_{eff} was positive and increased with the initial ratio of JD^{pa}. Thus, the observed shape transformation pathways corresponded well with the theoretical morphology diagrams based on m_{eff}.[33]

Two types of strikingly different morphologies were observed for multilamellar DSs. Irradiation resulted in the generation of high genus (*g* ~ 100) DSs with MLP with two distinct mesoscopic morphologies; nucleus-type and honeycomb-type MLPs for JD^{pa} ratios between 1—20% and 30—70%, respectively. Not only did the photocleavage of JD^{pa} result in the necessary increase in *m* but also in the local reduction of the hydrophilic repulsion allowing a multitude of adhesive contacts between apposing membranes that rapidly evolved into large pores. The adhesive contacts colocalized w-JD^{pa} whose non-bilayer forming nature supported the formation of pore precursors called IMI which transformed into ILA enabling the fusion and fission of the membranes. It was found that the content of JD^{pa} controlled the size and arrangement of the pores. Large pores with a narrow distribution of size organized in well-defined hexagonal arrays to minimize the membrane tension as demonstrated by FFT. The size and the separation of these pores followed an inverse relation with the content of JD^{pa}.

All smectic-ordered DSs followed the same type of transformation, the formation of outward-pointing buds at the mother DS's periphery which evolved into the first generation of daughter DSs. Further irradiation led to additional generations until all bilayers were consumed. We proposed that the mechanism was based on a combination of the mechanisms for uni- and multilamellar DSs involving the fusion of consecutive bilayers and the increase of m_{eff} to generate out-buds. Remarkably, an analysis of the size distribution and the neck stability support the model.

In summary, this work demonstrated that changes in the topology in even a small percentage of the amphiphiles forming vesicles can have drastic effects on the evolution of their shape. Various shape transformations observed here are ubiquitous in cells and their organelles but did not require any active cellular machinery. Thus, this work lays the foundation for the development of protocellular models to mimic and study membrane transformations, transport, and more complex mechanisms associated solely to living matter.

Conflicts of interest

There are no conflicts to declare.

Acknowledgments

References

1. R. Lipowsky, *Biol. Chem.*, 2014, **395**, 253-274.
2. J. Bigay and B. Antonny, *Dev. Cell*, 2012, **23**, 886-895.
3. H. T. McMahon and E. Boucrot, *J. Cell Sci.*, 2015, **128**, 1065-1070.
4. H. T. McMahon and J. L. Gallop, *Nature*, 2005, **438**, 590-596.
5. B. Alberts, A. Johnson, J. Lewis, D. Morgan, M. Raff, K. Roberts and P. Walter, *Molecular Biology of the Cell, Sixth Edition*, Garland Science, Taylor&Francis Group. LLC, 2014.
6. J. H. Lorent, K. R. Leventhal, L. Ganesan, G. Rivera-Longsworth, E. Sezgin, M. Doktorova, E. Lyman and I. Leventhal, *Nat. Chem. Biol.*, 2020, **16**, 644-652.
7. H. F. Renard, L. Johannes and P. Morsomme, *Trends Cell Biol.*, 2018, **28**, 274-286.
8. J. C. Stachowiak, F. M. Brodsky and E. A. Miller, *Nat. Cell Biol.*, 2013, **15**, 1019-1027.
9. K. Simons and G. van Meer, *Biochemistry*, 1988, **27**, 6197-6202.
10. T. Harder, P. Scheiffele, P. Verkade and K. Simons, *J. Cell Biol.*, 1998, **141**, 929-942.
11. D. Lingwood and K. Simons, *Science*, 2010, **327**, 46-50.
12. E. Sezgin, I. Leventhal, S. Mayor and C. Eggeling, *Nat. Rev. Mol. Cell Biol.*, 2017, **18**, 361-374.
13. K. Simons and E. Ikonen, *Nature*, 1997, **387**, 569-572.
14. R. Mercier, Y. Kawai and J. Errington, *Cell*, 2013, **152**, 997-1007.
15. S. Kretschmer, K. A. Ganzinger, H. G. Franquelim and P. Schwille, *BMC Biol.*, 2019, **17**, 43.
16. P. L. Luisi, T. P. de Souza and P. Stano, *J. Phys. Chem. B*, 2008, **112**, 14655-14664.
17. O. G. Mouritsen, *Eur. J. Lipid Sci. Technol.*, 2011, **113**, 1174-1187.
18. P. Walde, K. Cosentino, H. Engel and P. Stano, *Chembiochem*, 2010, **11**, 848-865.

19. E. Rideau, R. Dimova, P. Schwille, F. R. Wurm and K. Landfester, *Chem. Soc. Rev.*, 2018, **47**, 8572-8610.

20. R. Dimova, S. Aranda, N. Bezlyepkina, V. Nikolov, K. A. Riske and R. Lipowsky, *J. Phys.: Condens. Matter*, 2006, **18**, S1151-1176.

21. R. Dimova, *Annu. Rev. Biophys.*, 2019, **48**, 93-119.

22. C. LoPresti, H. Lomas, M. Massignani, T. Smart and G. Battaglia, *J. Mater. Chem.*, 2009, **19**, 3576.

23. D. E. Discher and A. Eisenberg, *Science*, 2002, **297**, 967-973.

24. G. Battaglia and A. J. Ryan, *J. Am. Chem. Soc.*, 2005, **127**, 8757-8764.

25. G. Battaglia and A. J. Ryan, *Angew. Chem., Int. Ed. Engl.*, 2006, **45**, 2052-2056.

26. G. Battaglia, S. Tomas and A. J. Ryan, *Soft Matter*, 2007, **3**, 470-475.

27. F. Itel, M. Chami, A. Najer, S. Lörcher, D. Wu, I. A. Dinu and W. Meier, *Macromolecules*, 2014, **47**, 7588-7596.

28. T. P. Smart, O. O. Mykhaylyk, A. J. Ryan and G. Battaglia, *Soft Matter*, 2009, **5**, 3607.

29. R. Lipowsky, *Nature*, 1991, **349**, 475-481.

30. R. Lipowsky and E. Sackmann, *Structure and Dynamics of Membranes*, Elsevier, 1995.

31. K. Berndl, J. Kas, R. Lipowsky, E. Sackmann and U. Seifert, *Europhys. Lett.*, 1990, **13**, 659-664.

32. U. Seifert, K. Berndl and R. Lipowsky, *Phys. Rev. A*, 1991, **44**, 1182-1202.

33. R. Lipowsky, From membranes to membrane machines, Sitges, Barcelona, Spain, 1999.

34. H. G. Dobereiner, E. Evans, M. Kraus, U. Seifert and M. Wortis, *Phys. Rev. E*, 1997, **55**, 4458-4474.

35. L. Miao, U. Seifert, M. Wortis and H. G. Dobereiner, *Phys. Rev. E: Stat. Phys., Plasmas, Fluids, Relat. Interdiscip. Top.*, 1994, **49**, 5389-5407.

36. R. E. Waugh, J. Song, S. Svetina and B. Zeks, *Biophys. J.*, 1992, **61**, 974-982.

37. E. Evans and A. Yeung, *Chem. Phys. Lipids*, 1994, **73**, 39-56.

38. S. Svetina and B. Zeks, *Eur. Biophys. J.*, 1989, **17**, 101-111.

39. E. A. Evans, *Biophys. J.*, 1974, **14**, 923-931.

40. U. Seifert, *Adv. Phys.*, 1997, **46**, 13-137.

41. E. Farge and P. F. Devaux, *J. Phys. Chem.*, 1993, **97**, 2958-2961.

42. M. Mally, B. Bozic, S. V. Hartman, U. Klancnik, M. Mur, S. Svetina and J. Derganc, *RSC Adv.*, 2017, **7**, 36506-36515.

43. K. Oglecka, J. Sanborn, A. N. Parikh and R. S. Kraut, *Front. Membr. Physiol. Membr. Biophys.*, 2012, **3**, 120.

44. I. Budin, A. Debnath and J. W. Szostak, *J. Am. Chem. Soc.*, 2012, **134**, 20812-20819.

45. V. N. Georgiev, A. Grafmuller, D. Bleger, S. Hecht, S. Kunstmann, S. Barbirz, R. Lipowsky and R. Dimova, *Adv. Sci. (Weinheim, Ger.)*, 2018, **5**, 1800432.

46. A. Seoane, R. J. Brea, A. Fuertes, K. A. Podolsky and N. K. Devaraj, *J. Am. Chem. Soc.*, 2018, **140**, 8388-8391.

47. R. J. Brea, A. K. Rudd and N. K. Devaraj, *Proc. Natl. Acad. Sci. U. S. A.*, 2016, **113**, 8589-8594.

48. M. D. Hardy, J. Yang, J. Selimkhanov, C. M. Cole, L. S. Tsimring and N. K. Devaraj, *Proc. Natl. Acad. Sci. U. S. A.*, 2015, **112**, 8187-8192.

49. T. Hamada, Y. T. Sato, K. Yoshikawa and T. Nagasaki, *Langmuir*, 2005, **21**, 7626-7628.

50. C. Pernpeintner, J. A. Frank, P. Urban, C. R. Roeske, S. D. Pritzl, D. Trauner and T. Lohmuller, *Langmuir*, 2017, **33**, 4083-4089.

51. M. Fossati, B. Goud, N. Borgese and J. B. Manneville, *Cell Logist.*, 2014, **4**, e29087.

52. K. P. Sinha, S. Gadkari and R. M. Thaokar, *Soft Matter*, 2013, **9**, 7274.

53. P. Bassereau, R. Jin, T. Baumgart, M. Deserno, R. Dimova, V. A. Frolov, P. V. Bashkirov, H. Grubmuller, R. Jahn, H. J. Risselada, L. Johannes, M. M. Kozlov, R. Lipowsky, T. J. Pucadyil, W. F. Zeno, J. C. Stachowiak, D. Stamou, A. Breuer, L. Lauritsen, C. Simon, C. Sykes, G. A. Voth and T. R. Weikl, *J. Phys. D: Appl. Phys.*, 2018, **51**.

54. Z. T. Graber, Z. Shi and T. Baumgart, *Phys. Chem. Chem. Phys.*, 2017, **19**, 15285-15295.

55. I. Tsafrir, Y. Caspi, M. A. Guedeau-Boudeville, T. Arzi and J. Stavans, *Phys. Rev. Lett.*, 2003, **91**, 138102.

56. I. Tsafrir, D. Sagi, T. Arzi, M. A. Guedeau-Boudeville, V. Frette, D. Kandel and J. Stavans, *Phys. Rev. Lett.*, 2001, **86**, 1138-1141.

57. J. Steinkuhler, R. L. Knorr, Z. Zhao, T. Bhatia, S. M. Bartelt, S. Wegner, R. Dimova and R. Lipowsky, *Nat. Commun.*, 2020, **11**, 905.

58. J. Agudo-Canalejo and R. Lipowsky, *Nano Lett.*, 2015, **15**, 7168-7173.

59. A. H. Bahrami, M. Raatz, J. Agudo-Canalejo, R. Michel, E. M. Curtis, C. K. Hall, M. Gradzielski, R. Lipowsky and T. R. Weikl, *Adv. Colloid Interface Sci.*, 2014, **208**, 214-224.

60. S. Dasgupta, T. Auth and G. Gompper, *Soft Matter*, 2013, **9**, 5473-5482.

61. N. Y. Kostina, K. Rahimi, Q. Xiao, T. Haraszti, S. Dedisch, J. P. Spatz, U. Schwaneberg, M. L. Klein, V. Percec, M. Moller and C. Rodriguez-Emmenegger, *Nano Lett.*, 2019, **19**, 5732-5738.

62. U. Bernchou, J. Brewer, H. S. Midtiby, J. H. Ipsen, L. A. Bagatolli and A. C. Simonsen, *J. Am. Chem. Soc.*, 2009, **131**, 14130-14131.

63. R. Goetz, G. Gompper and R. Lipowsky, *Phys. Rev. Lett.*, 1999, **82**, 221-224.

64. J. M. Holopainen, M. I. Angelova and P. K. J. Kinnunen, *Biophys. J.*, 2000, **78**, 830-838.

65. A. Bhattacharya, R. J. Brea, H. Niederholtmeyer and N. K. Devaraj, *Nat. Commun.*, 2019, **10**, 300.

66. Q. Xiao, S. S. Yadavalli, S. Zhang, S. E. Sherman, E. Fiorin, L. da Silva, D. A. Wilson, D. A. Hammer, S. Andre, H. J. Gabius, M. L. Klein, M. Goulian and V. Percec, *Proc. Natl. Acad. Sci. U. S. A.*, 2016, **113**, E1134-1141.

67. M. Peterca, V. Percec, P. Leowanawat and A. Bertin, *J. Am. Chem. Soc.*, 2011, **133**, 20507-20520.

68. S. Zhang, H. J. Sun, A. D. Hughes, R. O. Moussodia, A. Bertin, Y. Chen, D. J. Pochan, P. A. Heiney, M. L. Klein and V. Percec, *Proc. Natl. Acad. Sci. U. S. A.*, 2014, **111**, 9058-9063.

69. V. Percec, D. A. Wilson, P. Leowanawat, C. J. Wilson, A. D. Hughes, M. S. Kaucher, D. A. Hammer, D. H. Levine, A. J. Kim, F. S. Bates, K. P. Davis, T. P. Lodge, M. L. Klein, R. H. DeVane, E. Aqad, B. M. Rosen, A. O. Argintaru, M. J. Sienkowska, K. Rissanen, S. Nummelin and J. Ropponen, *Science*, 2010, **328**, 1009-1014.

70. S. Zhang, H. J. Sun, A. D. Hughes, B. Draghici, J. Lejnieks, P. Leowanawat, A. Bertin, L. Otero De Leon, O. V. Kulikov, Y. Chen, D. J. Pochan, P. A. Heiney and V. Percec, *ACS Nano*, 2014, **8**, 1554-1565.

71. S. S. Yadavalli, Q. Xiao, S. E. Sherman, W. D. Hasley, M. L. Klein, M. Goulian and V. Percec, *Proc. Natl. Acad. Sci. U. S. A.*, 2019, **116**, 744-752.

72. S. Li, B. Xia, B. Javed, W. D. Hasley, A. Melendez-Davila, M. Liu, M. Kerzner, S. Agarwal, Q. Xiao, P. Torre, J. G. Bermudez, K. Rahimi, N. Y. Kostina, M. Moller, C. Rodriguez-Emmenegger, M. L. Klein, V. Percec and M. C. Good, *ACS Nano*, 2020, **14**, 7398-7411.

73. C. E. Forkner, L. S. Zia and C. T. Teng, *Chin. Med. J.*, 1936, **50**, 1191-1194.

74. R. J. Pulvertaft, *J. Clin. Pathol.*, 1949, **2**, 281-283.

75. P.-G. de Gennes, *Angew. Chem., Int. Ed. Engl.*, 1992, **31**, 842-845.

76. F. Brochard and J. F. Lennon, *J. Phys.*, 1975, **36**, 1035-1047.

77. M. Antonietti and S. Förster, *Adv. Mat.*, 2003, **15**, 1323-1333.

78. D. H. Rich and S. K. Gurwara, *J. Am. Chem. Soc.*, 1975, **97**, 1575-1579.

79. B. Chandra, S. Mallik and D. K. Srivastava, *Chem. Commun.*, 2005, **2005**, 3021-3023.

80. P. Sunthar and S. M. Phapal, 2015.

81. V. Guida, *Adv. Colloid Interface Sci.*, 2010, **161**, 77-88.

82. D. D. Lasic, *Biochem. J.*, 1988, **256**, 1-11.

83. P. L. Luisi, *The emergence of Life. From Chemical Origins to Synthetic Biology*, Cambridge University Press: Cambridge, 2016.

84. J. R. Bruckner and F. Giesselmann, *Crystals*, 2019, **9**, 568.

85. P. G. Petrov, J. B. Lee and H. G. Dobereiner, *Europhys. Lett.*, 1999, **48**, 435-441.

86. E. Boroske, M. Elwenspoek and W. Helfrich, *Biophys. J.*, 1981, **34**, 95-109.

87. F. Brochard-Wyart, P. G. de Gennes and O. Sandre, *Physica A*, 2000, **278**, 32-51.

88. E. Karatekin, O. Sandre, H. Guitouni, N. Borghi, P.-H. Puech and F. Brochard-Wyart, *Biophys. J.*, 2003, **84**, 1734-1749.

89. W. T. Gozdz, *J. Chem. Phys.*, 2011, **134**, 024110.

90. R. Dimova and M. Marques, *The Giant Vesicle Book* CRC Press, Taylor & Francis Ltd., 2019.

91. H. Lodish, A. Berk, S. L. Zipursky, P. Matsudaira, D. Baltimore and J. Darnell, *Molecular Cell Biology*, W. H. Freeman and Company, 4th edn., 2000.

92. C. G. Palivan, R. Goers, A. Najer, X. Zhang, A. Car and W. Meier, *Chem. Soc. Rev.*, 2016, **45**, 377-411.

93. O. Sandre, Université Pierre & Marie Curie-Paris 6, 2000.

94. W. T. Góźdź, in *Advances in Planar Lipid Bilayers and Liposomes*, Elsevier, 2009, vol. 10, pp. 29-64.

95. A. A. Reinecke and H.-G. Döbereiner, *Langmuir*, 2003, **19**, 605-608.

96. H.-G. Döbereiner, *Curr. Opin. Colloid Interface Sci.*, 2000, **5**, 256-263.

97. X. Bian, S. Litvinov and P. Koumoutsakos, *Computer Methods in Applied Mechanics and Engineering*, 2020, **359**, 112758.

98. O. Sandre, L. Moreaux and F. Brochard-Wyart, *Proc. Natl. Acad. Sci. U. S. A.*, 1999, **96**, 10591-10596.

99. R. M. Raphael, R. E. Waugh, S. Svetina and B. Zeks, *Phys. Rev. E: Stat., Nonlinear, Soft Matter Phys.*, 2001, **64**, 051913.

100. T. Bhatia, S. Christ, J. Steinkuhler, R. Dimova and R. Lipowsky, *Soft Matter*, 2020, **16**, 1246-1258.

101. C. K. Haluska, W. T. Gozdz, H. G. Dobereiner, S. Forster and G. Gompper, *Phys. Rev. Lett.*, 2002, **89**, 238302.

102. K.-i. Akashi and H. Miyata, *J. Phys. Soc. Jpn.*, 2010, **79**, 064801.

103. R. Lipowsky and E. Sackmann, *Structure and Dynamics of Membranes. From Cells to Vesicles*, Elsevier Science, 1995.

104. X. Michalet, D. Bensimon and B. Fourcade, *Phys. Rev. Lett.*, 1994, **72**, 168-171.

105. S. W. Hui, T. P. Stewart, L. T. Boni and P. L. Yeagle, *Science*, 1981, **212**, 921-923.

106. D. P. Tieleman, H. Leontiadou, A. E. Mark and S. J. Marrink, *J. Am. Chem. Soc.*, 2003, **125**, 6382-6383.

107. J. Du and Y. Chen, *Angew. Chem., Int. Ed. Engl.*, 2004, **43**, 5084-5087.

108. D. P. Siegel, *Biophys. J.*, 1984, **45**, 399-420.

109. H. Ellens, D. P. Siegel, D. Alford, P. L. Yeagle, L. Boni, L. J. Lis, P. J. Quinn and J. Bentz, *Biochemistry*, 1989, **28**, 3692-3703.

110. J. K. Kim, E. Lee, Y. B. Lim and M. Lee, *Angew. Chem., Int. Ed. Engl.*, 2008, **47**, 4662-4666.

111. H. Noguchi, *Biophys. J.*, 2016, **111**, 824-831.

112. M. Torbati, T. P. Lele and A. Agrawal, *Proc. Natl. Acad. Sci. U. S. A.*, 2016, **113**, 11094-11099.

113. R. P. Rand and V. A. Parsegian, *Biochim. Biophys. Acta, Rev. Biomembr.*, 1989, **988**, 351-376.

114. R. G. Horn, *Biochim. Biophys. Acta, Biomembr.*, 1984, **778**, 224-228.

115. R. Lipowsky and E. Sackmann, *Structure and Dynamics of Membranes. Generic and Specific Interactions*, Elsevier Science, 1995.

116. S. Ohki, *J. Membr. Biol.*, 1984, **77**, 265-275.

117. P. R. Cullis and M. J. Hope, *Nature*, 1978, **271**, 672-674.

118. D. P. Siegel, *Biophys. J.*, 1986, **49**, 1155-1170.

119. D. P. Siegel, J. L. Burns, M. H. Chestnut and Y. Talmon, *Biophys. J.*, 1989, **56**, 161-169.

120. M. Wang, A. M. Mihut, E. Rieloff, A. P. Dabkowska, L. K. Mansson, J. N. Immink, E. Sparr and J. J. Crassous, *Proc. Natl. Acad. Sci. U. S. A.*, 2019, **116**, 5442-5450.

121. T. Auth and G. Gompper, *Phys. Rev. E: Stat., Nonlinear, Soft Matter Phys.*, 2009, **80**, 031901.